Chemical Engineering Journal 402 (2020) 126161

Contents lists available at ScienceDirect

Chemical Engineering Journal

journal homepage: www.elsevier.com/locate/cej

A sunlight-responsive and robust anti-icing/deicing coating based on the amphiphilic materials

Hongshuang Guo[a,b,c], Min Liu[a,b,c], Changhai Xie[a,b,c], Yingnan Zhu[a,b,c], Xiaojie Sui[a,b,c], Chiyu Wen[a,b,c], Qingsi Li[a,b,c], Weiqiang Zhao[a,b,c], Jing Yang[a,b,c,*], Lei Zhang[a,b,c,*]

[a] Department of Biochemical Engineering, School of Chemical Engineering and Technology, Tianjin University, Tianjin 300350, PR China
[b] Qingdao Institute for Marine Technology of Tianjin University, Qingdao 266235, PR China
[c] School of Chemical Engineering and Technology, Frontier Science Center for Synthetic Biology and Key Laboratory of Systems Bioengineering (MOE), Tianjin University, Tianjin 300350, PR China

HIGHLIGHTS

- A novel anti-icing/deicing coating based on the amphiphilic materials.
- The coating can be formed in a simple way.
- The coating shows excellent sunlight-responsive anti-icing/deicing performance in outdoor.

GRAPHICAL ABSTRACT

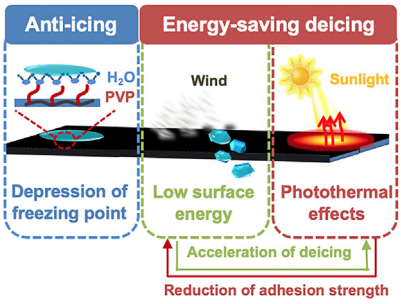

ARTICLE INFO

Keywords:
Anti-icing/deicing coating
Sunlight-responsive
Amphiphilic block copolymer
Nanocarbon fibers
Robustness

ABSTRACT

Ice accretion on airplane surfaces, power lines, or wind turbines can cause operational difficulties and disastrous events. Great efforts have been made to develop environmentally-friendly anti-icing or deicing surfaces over the last several decades, but a high-efficient, robust, and energy-saving surface for both anti-icing and deicing still remains a challenge. Herein, a sunlight-responsive and robust anti-icing/deicing coating is designed by integrating photothermogenic nanocarbon fibers with an amphiphilic material, which is based on hydrophobic polydimethylsiloxane (PDMS) and hydrophilic polyvinylpyrrolidone (PVP) segments. The resultant coating represents an excellent and energy-saving anti-icing/deicing performance: a 34-fold increase of freezing delay time compared with control steel and ~18 KPa of ice adhesion strength enabling easy removal by a natural wind action, attributable to the intrinsic material properties (the ability of PVP to depress water freezing point and the low surface energy of PDMS). Moreover, nanocarbon fibers can further reduce the ice adhesion strength and endow the coating with a rapidly sunlight-sensitive photothermal deicing performance (up to 10 °C/min), presenting the superiority of outdoor applications especially for high-altitude equipment and vehicles. After 30 icing-deicing cycle, simulated acid rain (pH = 0) scouring, sand dropping, and 200 abrasion cycle tests, this coating also exhibits an extraordinary durability and robustness. This work makes a promising anti-icing and deicing coating for a large-scale operation and practical applications in particular outdoors.

* Corresponding authors at: Department of Biochemical Engineering, School of Chemical Engineering and Technology, Tianjin University, Tianjin 300350, PR China.
E-mail addresses: jing_yang@tju.edu.cn (J. Yang), lei_zhang@tju.edu.cn (L. Zhang).

https://doi.org/10.1016/j.cej.2020.126161
Received 31 January 2020; Received in revised form 29 June 2020; Accepted 30 June 2020
Available online 07 July 2020
1385-8947/ © 2020 Elsevier B.V. All rights reserved.

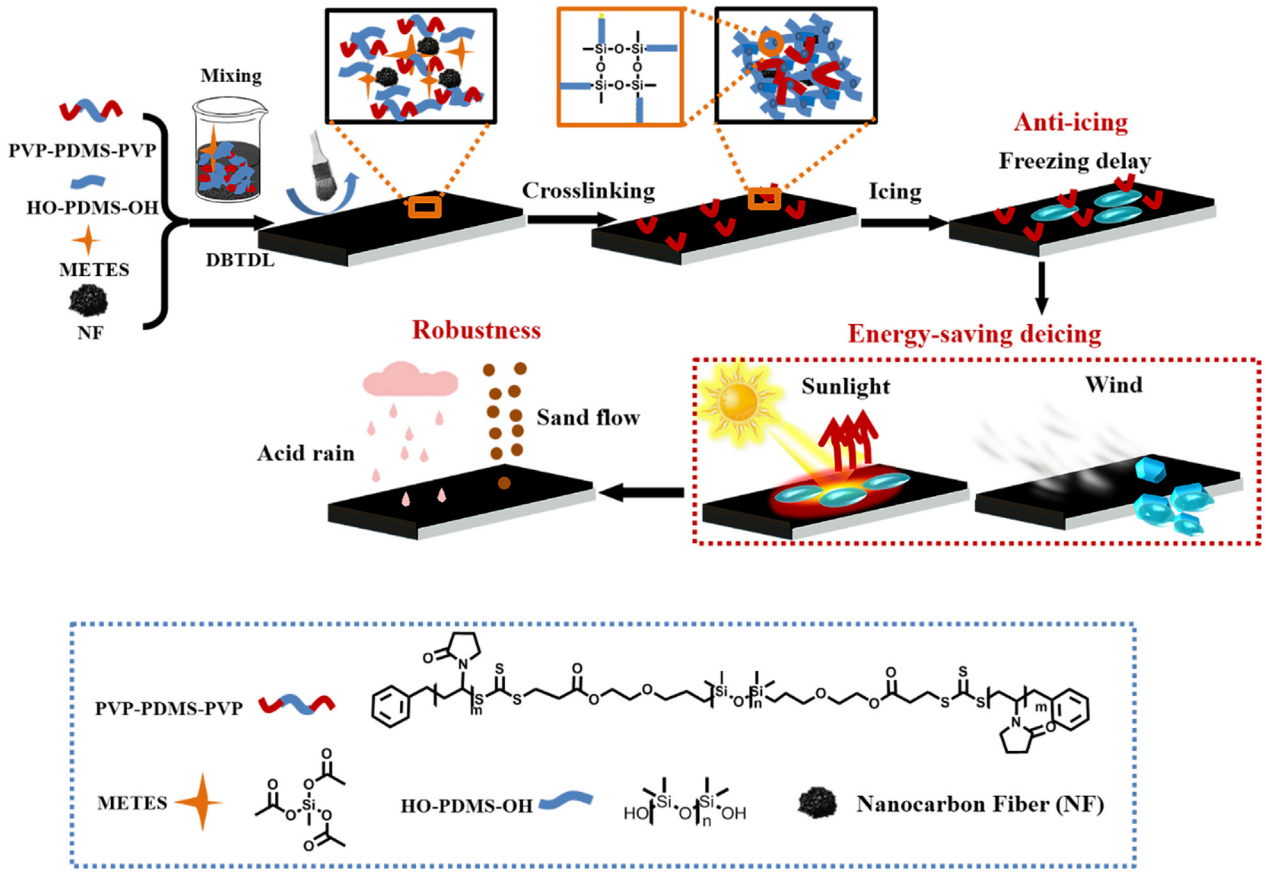

Fig. 1. Schematic illustration for development of the sunlight-responsive and robust anti-icing/deicing coating.

1. Introduction

Ice accretion on the surfaces of essential infrastructures including aircraft vehicles, wind turbines, power transmission lines, and highways, poses significant economic losses and safety challenges [1–9]. For example, ice-induced damage of transmission lines and towers in southern China leads to ~16 billion dollars in economic loss at the year of 2008. Another example is an air disaster, Continental Connection Flight 3407 from Newark to Buffalo crashed mainly due to ice accretion, resulting in all deaths in the airplane [10,11]. Current technologies and methods such as electrothermal deicing, hot-air deicing, and mechanical deicing have been used to alleviate the negative impact of ice accumulation, but they commonly suffer from low efficiency and energy consumption [12–15]. Other effective deicing methods based on chemical fluids and salts, which can depress the water freezing points but are harmful to environment as well as corrosive to metal [16].

Recently, passive anti-icing/ice-phobic surfaces to prevent ice formation or easily remove ice accretion represent an area of great interest, due to their significantly environmentally-friendly, energy-saving and safety properties [7,14,17–31]. For example, superhydrophobic surfaces based on the combination of micro/nanoscale texture and hydrophobic surface chemistry, possess the super-high water contact angles (≥150°) for effective water repellency [32–34]. Subsequently, a new class of functional materials, slippery liquid-infused porous surfaces (SLIPS) have been developed [14,26–28,35]. A textured solid is infiltrated by the lubricant to form a smooth liquid overlayer, which can significantly decrease ice adhesion strength. Although these surfaces are all promising, a robust and high-efficient anti-icing or deicing coating based on intrinsic material property for a large-scale operation in practice application is still highly desired.

Amphiphilic materials possess a bifunctional nature due to the incorporation of hydrophobic and hydrophilic segments, and are widely used as the antifouling and fouling-release coatings because the materials are capable of resisting fouling attachment and reducing biofouling adhesion strength. But there are few reports about amphiphilic anti-icing/deicing coatings [36–40], because they commonly exhibit a poor performance on efficiently and long-term anti-icing or deicing applications. In this work, we designed a novel sunlight-responsive amphiphilic coating, presenting an excellent anti-icing/deicing performance dependent on the intrinsic material properties: polyvinylpyrrolidone (PVP) possessing a high hydrophilicity to depress water freezing point and polydimethylsiloxane (PDMS) having a low surface energy to reduce ice adhesion strength [41,42]. Meanwhile, both PVP and PDMS possessed a superior stability and toughness under harsh conditions, to meet the challenge of long-term anti-icing coatings. Moreover, photothermogenic nanocarbon fibers (NFs) integrated with the amphiphilic coating could relieve the phase separation to further reduce the ice adhesion strength on coating surface, as well as endowing the coating with high thermogenesis efficiency only dependent on sunlight irradiation to harvest solar energy [43–45]. The penetration ability of sunlight would induce the ice melted at the ice-coating interface, resulting in quickly and easily deicing by gravity or wind action. This new design coating all basing on the cost-saving and tough materials presented an outstanding durability and robustness, even after 30 icing-deicing cycle, simulated acid rain scouring (pH = 0), sand dropping, and 200 abrasion cycle tests, benefiting a large-scale operation and practical applications in particular outdoors.

2. Materials and methods

2.1. Materials

Dihydroxyl-terminated polydimethylsiloxane (HO-PDMS-OH, M_W = 5600 or 26000 g mol^{-1}) was purchased from Dow Corning.

Dicyclohexylcarbodiimide (DCC), *tert*-butyl(chloro)dimethylsilane, 4-(dimethylamino)pyridine (DMAP) and methylsilanetriyl triacetate (METES) (96%) were all obtained from Heowns, Tianjin (China). N-vinylpyrrolidone (NVP, Acros, 99% stabilized with NaOH) was purified by distillation under reduced pressure to remove the inhibitors before use. Dibutyltin dilaurate (DBTDL, 97.5%) was purchased from j&k, China. 2, 2′-Azobis-(isobutyronitrile) (AIBN, Adamas) was purified by recrystallization from methanol three times before use. NFs (50 mesh, 270 μm) was purchased from Cangzhou Zhongli New Material Technology Co., Ltd. (China). All other reagents were used as received, and deionized water was used for all the experiments and tests.

2.2. Preparation of anti-icing/deicing coating

The preparation process of coating was presented in Fig. 1. Briefly, the PVP-PDMS-PVP polymer (preparation process described in Supporting Information) [46], METES, DBTDL and HO-PDMS-OH were dissolved in CH_2Cl_2 and mixed with NFs by an ultrasonic treatment for 10 min at room temperature. The obtained mixture was coated onto carbon steel plates or glasses. The resultant coatings were allowed to cure for 3 h at room temperature, followed by an additional 8 h in a vacuum oven at 70 °C to completely crosslinking and evaporate solvents. Four ratio coatings were prepared in this work and their mass ratios were listed in Table 1. The thickness of the coating was 0.2 mm. The coatings were named as PP5, PP5C5 and PP5C10. "PP" represented the amphiphilic PVP-PDMS coatings, "C" represented nanocarbon fibers, and"number" represented the mass percentages of the amphiphilic polymers or nanocarbon fibers.

2.3. Anti-icing properties

Icing delay time (DT) was performed on a cooling stage under N_2 atmosphere at a constant working temperature of −15 °C. The water droplets (6 μL) were placed on the coating surfaces by an injector needle tube, and tested in situ by a high speed CCD camera. The carbon steel plates or glasses were tightly attached to the cooling stage, and a certain time period was required for surface temperature equilibrium (−15 °C) before testing. The DT was defined as the time taken by the droplet contact with coating from transparency to non-transparency. Once the water droplet began to freeze, the transparent center of the water droplet vanished immediately due to the different reflectivity between water and ice. The room temperature was 20 ± 2 °C and the relative humidity was 50 ± 5% controlled by a humidifier.

2.4. Energy-saving deicing properties

The ice adhesion strength was measured by the method as described in previous literature [30,47]. The shear strength that was required to remove ice from the coating was considered as ice adhesion strength. Briefly: bottomless cuvettes were placed onto the coating surfaces and were filled with 450 μL water. The contact area on coating of each column was ~78.5 mm^2. To decrease the environment humidity, an organic glass box purged with N_2 was used to cover the cooling stage and the stage maintained at −15 °C for 4 h. A force transducer (Imada ZP-500 N, Japan) was mounted on a motion stage which moved forward at a rate of 0.5 mm/s to the cuvettes. The maximum force was recorded to calculate the ice adhesion strength by dividing the contact area between ice and coating surface. We obtained these average values and standard deviation from four parallel samples.

Table 1
The compositions of anti-icing/deicing coatings.

Sample	HO-PDMS-OH(g)	PVP-PDMS-PVP(g)	METES(g)	NFs(g)
PDMS	5	0	0.1	0
PP5	5	0.25	0.1	0
PP5C5	5	0.25	0.1	0.25
PP5C10	5	0.25	0.1	0.5

The sunlight-responsive deicing properties of coatings were tested by recording the melting time of ice on the surface with increasing temperatures. A glaze ice was prepared by spraying water micro-droplets (mimic freezing rain) onto the as-prepared samples at subzero temperatures, i.e. < −10 °C and RH ≈ 80%. In order to mimic the formation of glaze, all samples were further frozen under −20 °C and RH ≈ 70% conditions. Sunlight-responsive deicing tests were investigated in a < −5 °C and RH ≈ 70% environment, where the as-prepared samples were exposed to a sunlamp light (150 W) commonly used as a solar simulator source. A MT4 MAX infrared thermometer from Fluke Co., USA was used to measure the temperature. The coating surface temperatures were recorded and collected by an Infrared Radiation (IR) camera. The distances between the sunlamp and coating surfaces were 10, 15 and 20 cm, respectively.

2.5. Characterizations

FTIR spectra were recorded on a Bruker Tensor spectrometer (Bruker Optics, Germany) using attenuated total reflectance (ATR) mode from 4000 to 600 cm^{-1} with a resolution of 4 cm^{-1} and scanning times of 32. The surface morphology was examined by field emission scanning electron microscope (FE-SEM) (JSM7610F, Hitachi Ltd. Japan) and tapping mode atomic force microscopy (AFM) (CSPM5500A of Ben Yuan Ltd., China). AFM equipped with E-type vertical engage piezoelectric scanner and operated in a tapping mode at room temperature. The scanning range was 5 mm × 5 mm. The root-mean-square (RMS) roughness value was calculated on the obtained image. The water contact angles were measured by the sessile-drop method using an optical CA goniometry optical meter (Shanghai Zhongchen Digital Technology Apparatus Co. JC2000D1) with 5 μL of water droplets.

3. Results and discussion

3.1. Characterization of anti-icing/deicing coatings

Fig. 1 showed the typical fabricating procedures of the sunlight-responsive and robust anti-icing/deicing coating. The coating was prepared via a crosslinking process by METES, DBTDL and HO-PDMS-OH to form a network, as well as blending amphiphilic PVP-PDMS-PVP polymers. The coating was gradually formed by the condensation reaction of HO-PDMS-OH and Si-OH groups, generated by the hydrolysis of crosslinker METES in the presence of DBTDL as catalysts at 70 °C. Meanwhile, NFs were dispersed uniformly in pre-chemical reaction solution and embedded in the crosslinking networks.

The chemical structures of amphiphilic PVP-PDMS-PVP polymer, the pristine PDMS, PP5, PP5C5, and PP5C10 coating were identified by FTIR spectra in Fig. 2a. In the FTIR spectra of PVP-PDMS-PVP polymer, an absorption peak at 1000–1150 cm^{-1} was assigned to asymmetric stretching vibration of Si-O-Si. The peak at 795 cm^{-1} was attributed to Si-C bending vibration (a characteristic signal of PDMS). A wide peak at 3359–3657 cm^{-1} was attributed the water absorption of PVP due to its strong hydrophilicity, inducing a certain amount of water bound in the amphiphilic copolymer. The peak at 1660 cm^{-1} was stretching vibration of carboxyl group −CO− in the copolymer; 1270 cm^{-1} and 2962 cm^{-1} represented −–CN− and −CH-bond stretching vibration absorption peak, respectively [48]. In the spectra of amphiphilic coatings with or without NFs (PP5, PP5C5, and PP5C10), their absorption bands at 789 and 1083 cm^{-1} that were respectively assigned to Si-C and Si-O-Si stretching vibration presented to be stronger, and 2960 and 2858 cm^{-1} assigned to C−H were also obviously strengthened. In addition, the band of Si−O−Si groups in the range of 900–1100 cm^{-1} became a wider wavenumber. These results confirmed the condensation

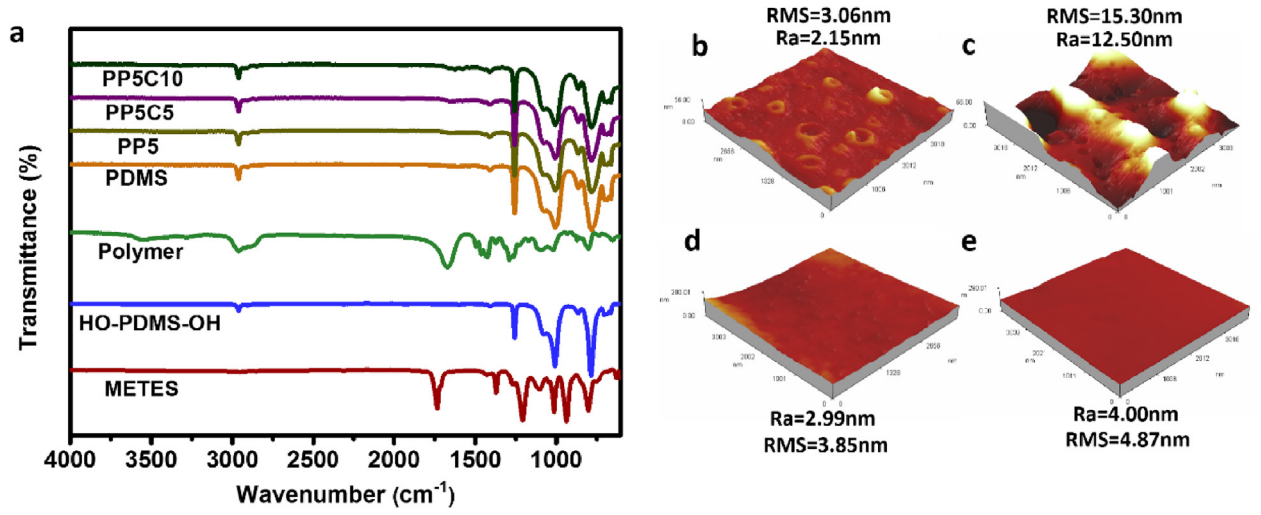

Fig. 2. (a) FTIR spectra of amphiphilic PVP-PDMS-PVP polymer, HO-PDMS-OH polymer, METES, PDMS, PP5, PP5C5, and PP5C10 coatings. The typical three-dimensional AFM height images of PDMS (b), PP5 (c), PP5C5 (d), and PP5C10 (e) coatings.

reaction between Si—OH and HO—PDMS—OH to form a crosslinking polymer network, and chemical structure of amphiphilic coating was not affected by the addition of NFs.

Next, SEM and AFM were used to study the surface topography and roughness structure of the coatings. In Fig. S1a and b, the SEM image of pristine PDMS coating showed a relatively smooth surface, while obvious micro/nanoscale vesicles appeared on the amphiphilic coating without NFs (PP5). This was probably due to the partial phase separation of hydrophilic segments in hydrophobic PDMS matrix. The NF-embedded PP5C5 and PP5C10 coatings presented the smoothness in Fig. S1c and d. Moreover, Fig. 2b-e showed the three-dimensional height images of coating surfaces using AFM, and the RMS values of PDMS, PP5, PP5C5, and PP5C10 coatings were 3.06 nm, 15.30 nm, 3.85 nm, and 4.87 nm, respectively. PP5 presented a rougher surface consistent with SEM images, while NF-embedded coatings showed the significantly increased smoothness that would contribute to reduce ice adhesion strength. Because NFs increased the hydrophobicity of coatings to relieve the phase separation.

With increasing time (0–300 s), water contact angles (WCAs) of these coatings were recorded under ambient conditions in Fig. S2. The results showed that the pristine PDMS coating possessed a hydrophobicity for large WCAs. In comparison, WCA of PP5 coating presented a significant decrease from 100° to 85° due to the hydrophilic PVP segments, while a slight decrease of WCAs on PP5C5 and PP5C10 coatings were attributable to the addition of hydrophobic NFs. Moreover, we calculated and studied surface free energies of these coatings according to the Owens-Wendt method, and the results are presented in Table 2 [49]. The surface energy of PP5C5 and PP5C10 coatings showed a slight increase with time, due to hydrophilic PVP segments beneficial to prolong the frozen time, but most values were less than 30 mN/m considered as a low surface energy.

Table 2
Contact angles and surface energies of the coatings.

	Water contact angle (°)	CH_2I_2 contact angle (°)	γ_{sv}^p (mN/m)	γ_{sv}^d (mN/m)	γ_{sv} (mN/m)
PDMS (0)	112	70	0.00	23.44	23.44
PDMS (1)	109	68	0.05	24.28	24.33
PDMS (2)	107	66	0.10	25.27	25.37
PDMS (3)	103	65	0.44	25.29	25.73
PP5 (0)	100	60	0.56	28.03	28.59
PP5 (1)	97	58	0.93	28.80	29.73
PP5 (2)	90	57	2.63	28.24	30.87
PP5 (3)	85	56	4.33	28.01	32.34
PP5C5 (0)	102	61	0.35	27.71	28.06
PP5C5 (1)	100	59	0.51	28.67	29.18
PP5C5 (2)	97	58	0.94	28.80	29.74
PP5C5 (3)	92	57	2.03	28.58	30.61
PP5C10 (0)	103	63	0.34	26.58	26.92
PP5C10 (1)	98	63	1.06	26.41	27.47
PP5C10 (2)	95	61	1.65	26.55	28.20
PP5C10 (3)	93	59	1.97	27.49	29.46

3.2. Anti-icing performance

In this work, the anti-icing property of coatings was evaluated by the representative test, crystallization delay of water droplets. Fig. S3 and 3 showed the water freezing process on different coatings compared to control steel and glass at −15 °C. The significantly decreased transparency of the droplet center represented the initiation of water freezing process. On the PP5, PP10 and PP15 coatings, water freezing initiated at 120 s, 148 s, and 154 s, respectively, all significantly longer than the frozen time of water droplets on the carbon steel (4 s), glass (8 s) and pristine PDMS coating (80 s), indicating that the addition of hydrophilic PVP could efficiently delay the frozen time. Fig. 3a-b demonstrated that PVP was able to effectively depress the water freezing points using a DSC test. Because PVP could strongly bound a large number of water molecules to inhibit hydrogen-bond network formation, which is directly associated with water crystallization [50–52]. To ensure the coating strength, PP5 was chosen to encapsulate the photothermogenic NFs. As shown in Fig. 3c, delay in the freezing of water drops on PP5C5 and PP5C10 coatings could achieve ~34 folds and ~38 folds compared to blank control steel, also longer than that of PP5 coating. These results indicated that the addition of NFs could also improve the anti-icing performance of amphiphilic coating, probably due to a more smoothness of NF-embedded coating surfaces.

3.3. Energy-saving deicing performance

In a subzero environment, the ice crystallization would always be formed and growth when a certain amount of supercooled water on the surfaces. So in this work, the ice adhesion strength was tested at −15 °C using a self-made measurement device, which was consisted of a cooling stage and a force transducer as depicted in Fig. 4a. As shown in Fig. 4b, the ice adhesion strength achieved up to ~600 KPa on the uncoated substrate, indicating the tight adhesion of ice with the carbon steel surface. When the substrate was coated by pristine PDMS with a low surface energy, the strength could be reduced to ~52.6 KPa, while ~43 KPa on PP5 coating, suggesting that the maintained low surface

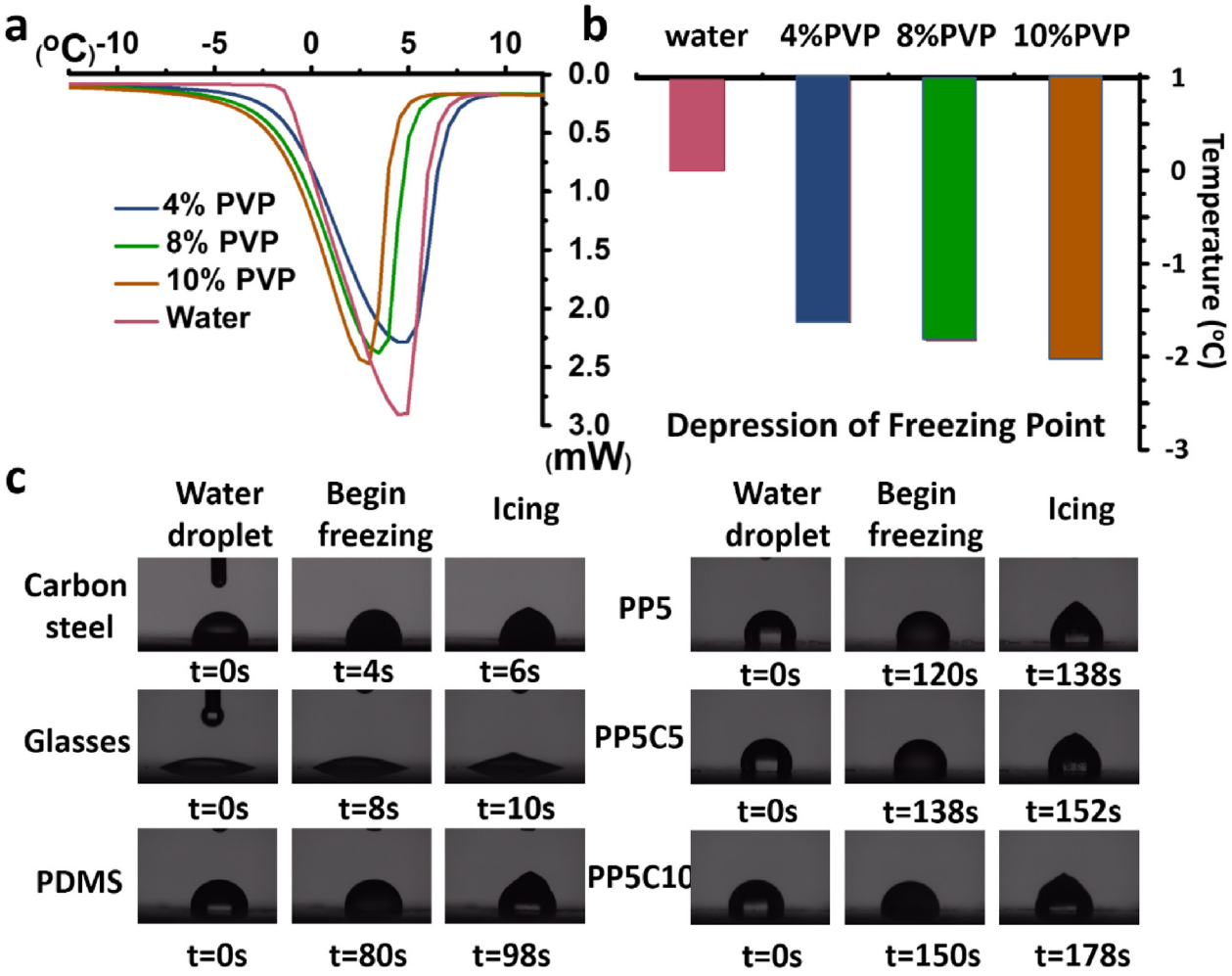

Fig. 3. (a) DSC melting thermograms and (b) freezing point depression of different concentrations of PVP. (c) Freezing process of water droplets on the control carbon steel, glass, pristine PDMS and amphiphilic coatings with or without NFs at −15 ˚C.

energy of amphiphilic coatings. Notably, the ice adhesion strength on NF-embedded PP5C5 coating surfaces was as low as ~18 KPa, exhibiting a superiority compared to many previously reported anti-icing coatings as presented in Fig. 4d. It has been reported that ice can be shaken off surfaces by natural wind action, gravity, or vibration if the adhesion strength is lower than 50 KPa [53], indicating the energy-saving deicing ability of PP5C5 coating. This result could be ascribed to a more smooth and lower surface energy coating based on NFs and PDMS, as demonstrated in Fig. 2d-e, minimizing the mechanical interlocking between the ice and surface texture.

The prolonged cycle durability is also important to the anti-icing coating, but difficult to some kinds of lubricating anti-icing surfaces [17]. As shown in Fig. 4c, the ice adhesion strength of PP5C5 coating was tested for 30 icing/deicing cycles in 40 days, and the results presented that it could maintained a stable low strength (~30 KPa) without obvious increase during 30 cycles. It could be attributed to the toughness of amphiphilic materials with NFs, and anti-icing/deicing capability of PP5C5 coating resulted from the intrinsic property of materials, instead of the artificial structure or infusing lubricants.

Sunlight is an infinite energy resource to infrastructures outdoor especially high-altitude aircraft vehicles. Meanwhile, natural sunlight containing the infrared light possesses high penetration capability to enable arrival at the ice-substrate interface through heavy moisture and thick ice layer. We designed a sunlight-sensitive coating based on photothermogenic NFs that could efficiently harvest and convert solar energy to heat for deicing, and NFs are cost-saving for a large-scale operation. Fig. 5a illustrated a simple photothermal experimental setup with a sunlamp for light illumination. Compared to other conventional heating sources, the utilization of sunlight required a more sensitive and effective material to light to-heat conversion. As shown in Fig. 5b-d, the temperatures on the different coatings were increased by simulated solar irradiation at ambient conditions. The coating without NFs (PDMS and PP5) showed a negligible increase of temperature during 5 min irradiation (25 ˚C to 26.7 ˚C or 27.6 ˚C) at 20 cm and 15 cm distance between sunlamp and coating surfaces. As expected, the increase of temperatures on PP5C5 and PP5C10 coating surfaces were much higher in same conditions, and surprisingly exceeded up to 9 ˚C only after 1 min irradiation at 10 cm distance. It could be observed that the temperatures of all coatings finally reached an equilibrium with the surrounding environment temperatures. In addition, outdoor experiment was also evaluated, and thermal images of the coatings under natural sunlight were collected by an Infrared Radiation (IR) camera in Fig. 5e and f. Under natural solar irradiation, pristine PDMS and PP5 coating surfaces achieved an equilibrium temperature at ~33 ˚C, while PP5C5 and PP5C10 coating temperatures could achieve up to ~48 ˚C. These results demonstrated that NF-embedded coatings could rapidly harvest solar energy and effectively convert to heat only depended on natural sunlight, indicating their energy-saving deicing property.

Next, photothermal deicing capability of the coatings was evaluated in Fig. 6. An ice layer was formed on the PDMS, PP5, PP5C5, and PP5C10 coatings to mimic ice accretion from freezing rain, as shown in Fig. 6b1-b4. Then, icing samples were placed under the sunlamp

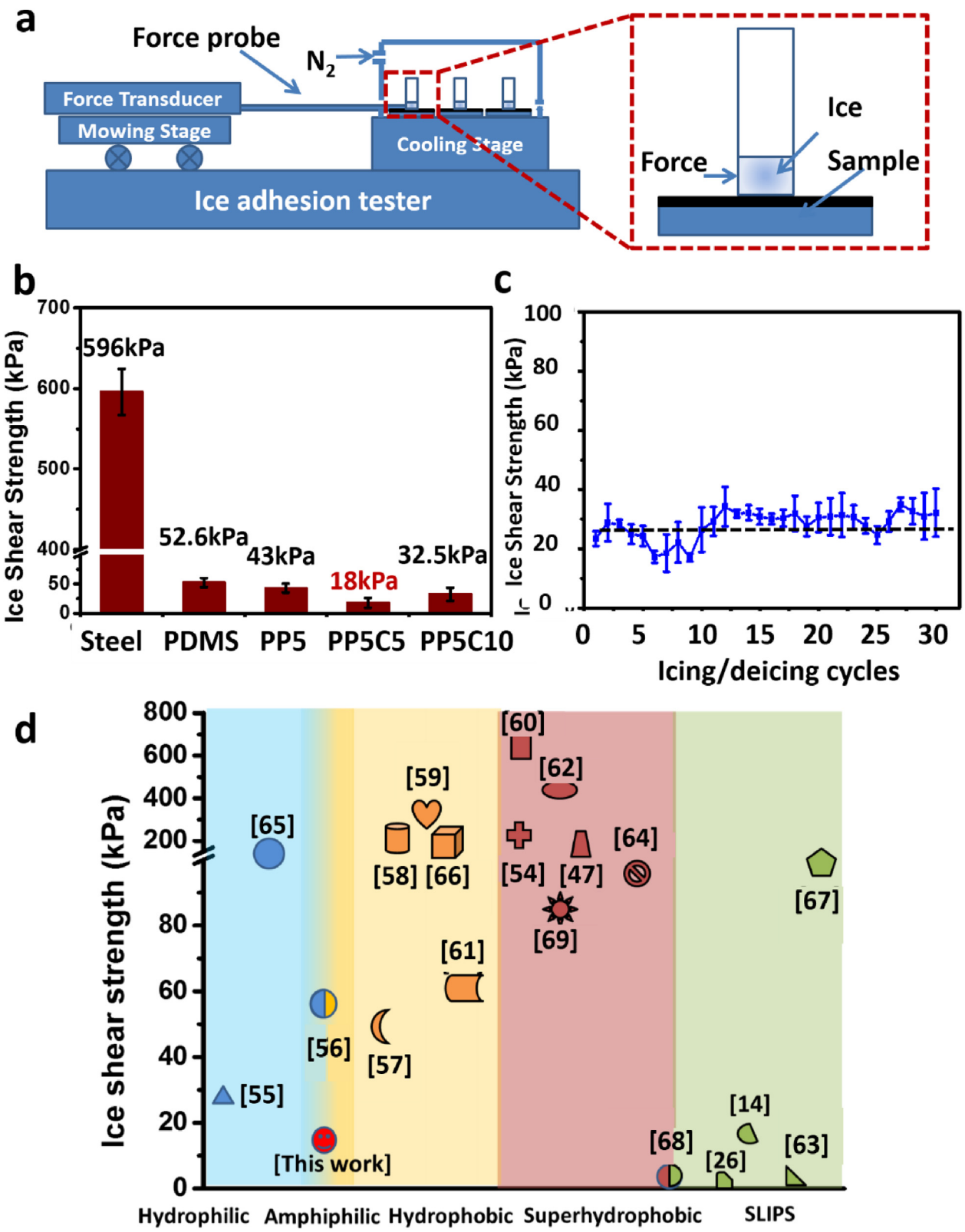

Fig. 4. (a) Schematic diagram of ice shear stress measurement. (b) Average ice adhesion strength on different samples. (c) Variation of ice adhesion strength on PP5C5 coating surface during 30 icing/deicing cycles. (d) The deicing capability of the coating prepared in this work and previously reported anti-icing coatings (Refer [14,26,47,54–69]). Color of the area represents the different types of recently reported ice-repellent surfaces.

irradiation, maintained in a supercooled environment below 0 °C. Fig. 6b5-b6 showed that the ice layer on PDMS and PP5 surfaces started to melt on layer surfaces, while melt at the location contact with the PP5C5 and PP5C10 coating with a much faster melting speed than PDMS and PP5 (Fig. 6b7). The totally melting time of ice layer was shown in Fig. 6c. PP5C5 (320 ± 28 s) and PP5C10 (318 ± 21 s) exhibited an almost twice melting speed as fast as PDMS (620 ± 28 s) and PP5 (595 ± 25 s). Moreover, the sunlight-responsive deicing

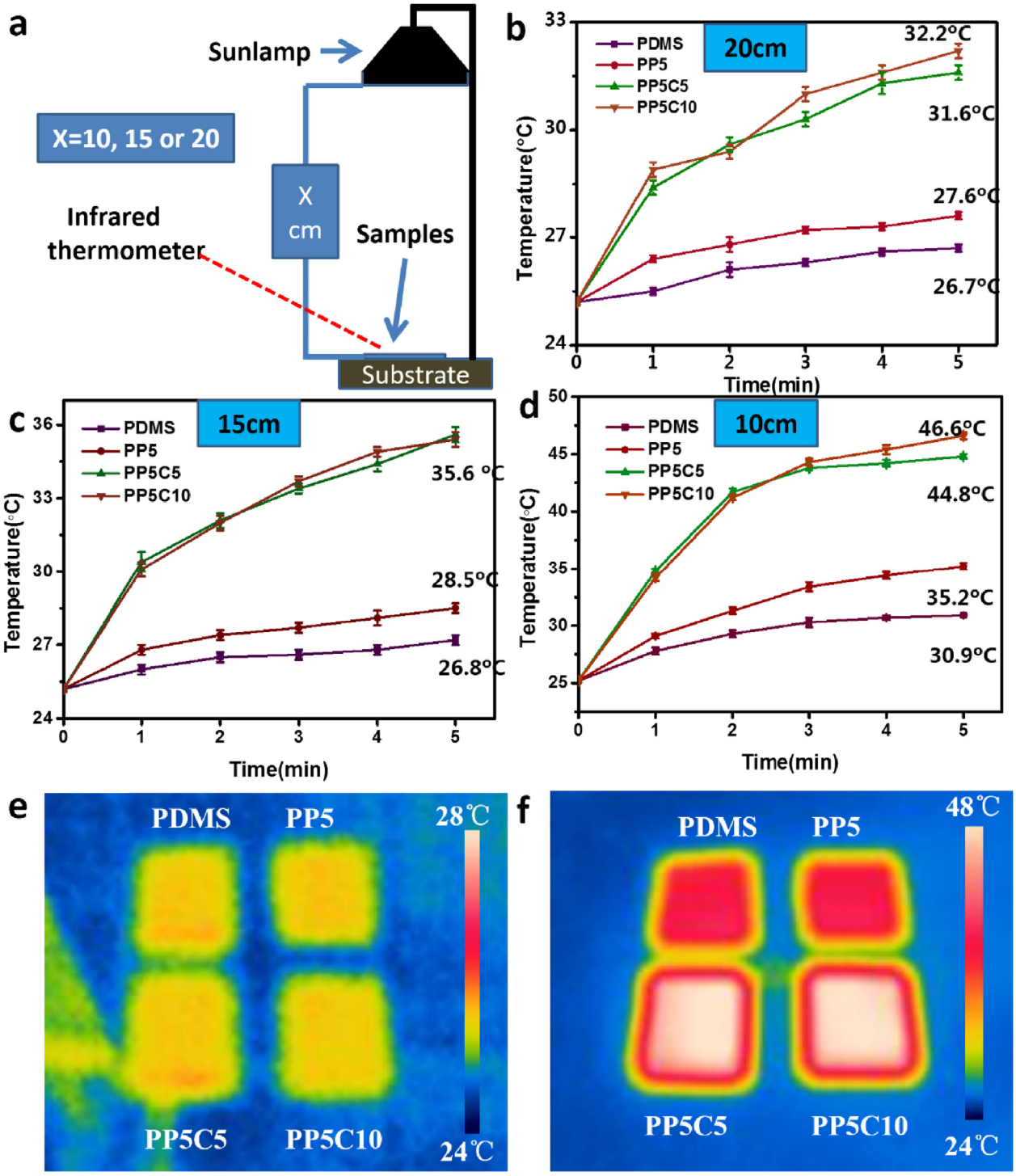

Fig. 5. (a) Photothermal experimental setup for light energy from a sunlamp (used as the solar simulator source). The surface temperatures were measured by a non-contact infrared thermometer. (b) (c) (d) The temperatures of sample surfaces under sunlamp irradiation (150 W) with different distances between sunlamp and sample surface. (e) (f) IR images of PDMS, PP5, PP5C5 and PP5C10 coatings under natural sunlight irradiation.

process of PP5C5 coating was depended on ice gravity and spent only 73 s as presented in Fig. 6d and Video S1, also consistent with the deicing time of a bulk ice (Fig. S4).

The energy-saving deicing property contributed to the penetration of sunlight through the ice, rapid sunlight-to-heat conversion induced by NFs for ice melting at substrate-ice interface, as well as the low ice adhesion strength caused by low surface energy of amphiphilic PVP-PDMS materials, leading to the shedding of ice dependent on its own gravity. This property is highly favorable to be applied in high-altitude equipment or vehicles.

3.4. Robustness of coating

Robustness of anti-icing or deicing coatings is extremely critical to infrastructures outside, which commonly suffer from a harsh environment. To evaluate the toughness and robustness of this coating, we performed HCl solution (pH = 0) scouring test to mimic artificial acid rain, as shown in Fig. 7a. PP5C5 coating maintained a low ice adhesion

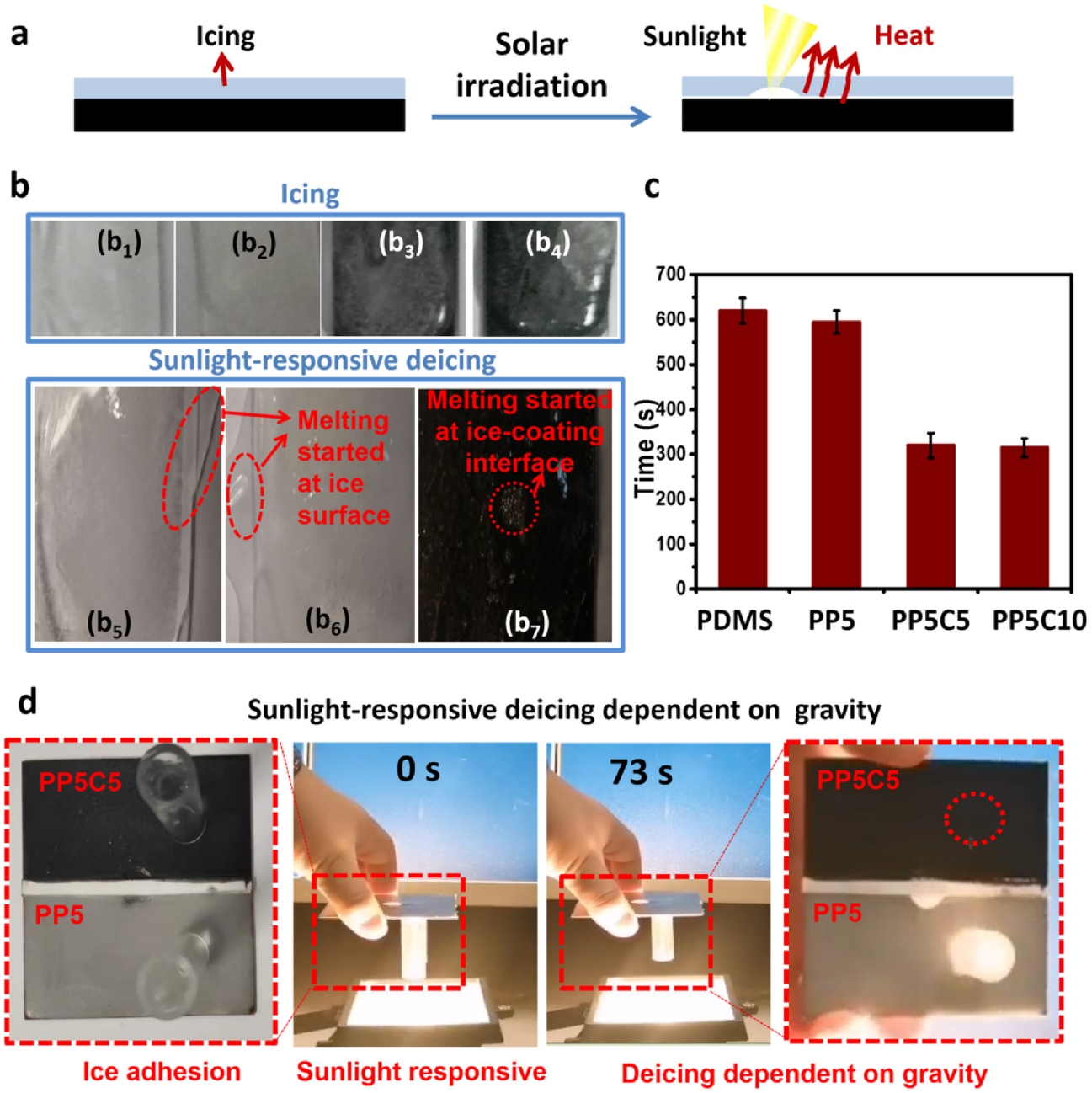

Fig. 6. (a) Schematic diagram of sunlight-responsive deicing test. (b1–b4) Photos of the ice layers and on PDMS, PP5, PP5C5, and PP5C10 coating surfaces. (b5) (b6) Photos of ice melting started at ice surfaces for PDMS and PP5 coatings (b7) and at ice-coating interface for PP5C5 (same as PP5C10). (c) The time taken by the ice layer melting totally under a sunlamp. (d) Sunlight-responsive deicing process dependent on ice gravity.

strength after impinging action by HCl solution jet (8 mm diameter) at ~1 m s^{-1} of total 1–3 L. Moreover, sand dropping test that can usually evaluate an abrasion-resistant substrate was used in this work (Fig. 7b) [70,71]. A large amount of sea sand (size, 100–300 mesh) fell down from a 50 cm height to the surface of PP5C5 sample at a 45°angle. The ice shear strength of the abraded surface presented a negligible increase during 30 min test. The surface morphology after HCl solution scouring and sand dropping tests also presented no obvious scratch or injury on the PP5C5 coating, as shown in Figure S1 e and f. In addition, after 200 abrasion cycles using a sandpaper, PP5C5 could still maintained an ice adhesion strength below 50 KPa (enabling removal by natural wind action), as presented in Fig. S5. The excellent washout resistance, acid tolerance, and abrasion resistance of this coating were related to the toughly chemical crosslinking based on all stable materials.

4. Conclusions

In summary, we designed a robust coating that possessed the unique property of effectively anti-icing and sunlight-responsive deicing. It integrated an amphiphilic PVP-PDMS material with photothermal nanocarbon fiber, and its anti-icing and deicing performance was dependent on intrinsic material properties: a significant freezing delay of anti-icing property was mainly attributable to the hydrophilicity of PVP, and the energy-saving deicing performance was attributable to a low surface energy of PDMS and a rapid sunlight-to-heat conversion of NFs. Furthermore, the results of icing/deicing cycle, simulated acid rain scouring, sand dropping, and abrasion cycle tests were demonstrated the excellent durability, robustness, and toughness of this coating. This work will be expected to promote the advancement of anti-icing/deicing materials in practical applications especially for outdoor

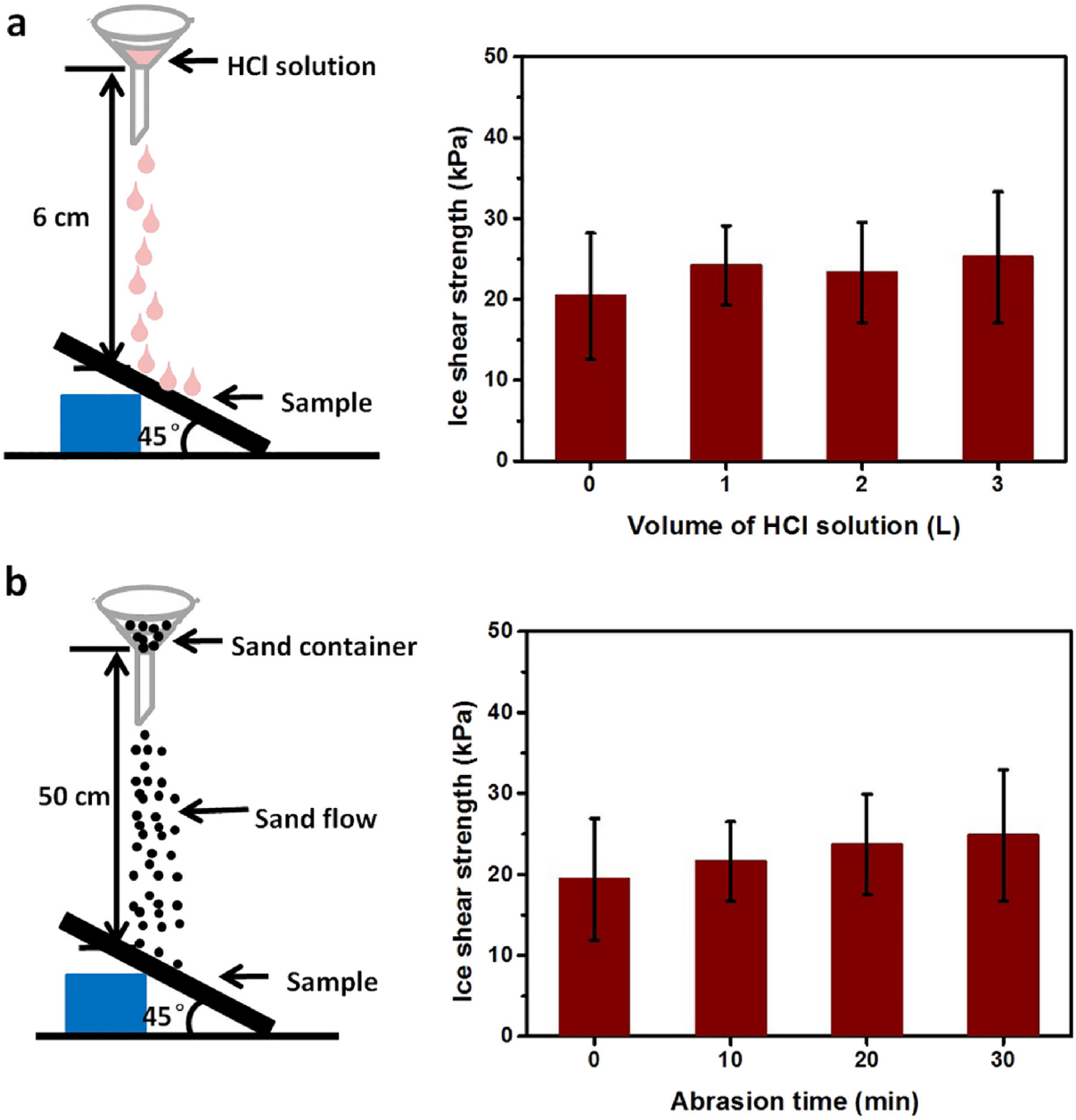

Fig. 7. Robustness evaluations: (a) Ice adhesion strength of PP5C5 coating scoured by the different volume of HCl solution (pH = 0). The distance between the drop falling location and sample surface is 6 cm. (b) Abrasion-resistant test using sand flow. The distance between the sand falling location and sample surface is 50 cm.

infrastructure.

Declaration of Competing Interest

The authors declare that they have no known competing financial interests or personal relationships that could have appeared to influence the work reported in this paper.

Acknowledgements

This research is supported by financial support from the Qingdao National Laboratory for Marine Science and Technology QNLM2016ORP0407, the National Natural Science Foundation of China (21621004, 21961132005, 21422605, 21908160), the Tianjin Natural Science Foundation, 18JCYBJC29500 and the China Postdoctoral Science Foundation 2019M651041.

Appendix A. Supplementary data

Supplementary data to this article can be found online at https://doi.org/10.1016/j.cej.2020.126161.

References

[1] A.J. Meuler, G.H. McKinley, R.E. Cohen, Exploiting topographical texture to impart icephobicity, ACS Nano. 4 (2010) 7048–7052.
[2] L.B. Boinovich, A.M. Emelyanenko, V.K. Ivanov, A.S. Pashinin, Durable icephobic coating for stainless steel, ACS Appl. Mater. Interfaces. 5 (2013) 2549–2554.
[3] A.G. Kraj, E.L. Bibeau, Phases of icing on wind turbine blades characterized by ice accumulation, Renew. Energy. 35 (2010) 966–972.
[4] Q. Li, Z. Guo, Fundamentals of icing and common strategies for designing biomimetic anti-icing surfaces, J. Mater. Chem. A. 6 (2018) 13549–13581.
[5] S.K. Thomas, R.P. Cassoni, C.D. MacArthur, Aircraft anti-icing and de-icing techniques and modeling, J. Aircraft. 33 (1996) 841–854.
[6] J. Marwitz, M. Politovich, B. Bernstein, F. Ralph, P. Neiman, R. Ashenden, J. Bresch, Meteorological conditions associated with the ATR72 aircraft accident near Roselawn, Indiana, on 31 October 1994, B. Am. Meteorol. Soc. 78 (1997) 41–52.
[7] J. Lv, Y. Song, L. Jiang, J. Wang, Bio-inspired strategies for anti-icing, ACS Nano. 8

(2014) 3152–3169.
[8] N. Dalili, A. Edrisy, R. Carriveau, A review of surface engineering issues critical to wind turbine performance, Renew. Sust. Energ. Rev. 13 (2009) 428–438.
[9] O. Parent, A. Ilinca, Anti-icing and de-icing techniques for wind turbines: critical review, Cold Reg. Sci. Technol. 65 (2011) 88–96.
[10] F.R. Mosher, D. Schaum, C. Herbster, T. Guinn, Analysis of causes of icing conditions which contributed to the crash of continental flight 3407. Presented at 14th Conference on Aviation, Range, and Aerospace Meteor-ology, Atlanta, GA, 1721 January, (2010).
[11] C.C. Liu, J. Liu, Ice accretion cause and mechanism of glaze on wires of power transmission lines, Adv. Mater. Res. 189–193 (2011) 3238–3242.
[12] P. Guo, M. Wen, L. Wang, Y. Zheng, Strong anti-ice ability of nanohairs over micro-ratchet structures, Nanoscale. 6 (2014) 3917–3920.
[13] M. Ruan, W. Li, B. Wang, B. Deng, F. Ma, Z. Yu, Preparation and anti-icing behavior of superhydrophobic surfaces on aluminum alloy substrates, Langmuir. 29 (2013) 8482–8491.
[14] P. Kim, T.-S. Wong, J. Alvarenga, M.J. Kreder, W.E. Adorno-Martinez, J. Aizenberg, Liquid-infused nanostructured surfaces with extreme anti-ice and anti-frost performance, ACS Nano. 6 (2012) 6569–6577.
[15] Y. Wang, N. Hudson, R. Pethrick, C. Schaschke, Poly (acrylic acid)–poly (vinyl pyrrolidone)-thickened water/glycol de-icing fluids, Cold Reg. Sci. Technol. 101 (2014) 24–30.
[16] D.M. Ramakrishna, T. Viraraghavan, Environmental impact of chemical deicers – A review, Water, Air, Soil Pollut. 166 (2005) 49–63.
[17] K. Golovin, S.P.R. Kobaku, D.H. Lee, E.T. DiLoreto, J.M. Mabry, A. Tuteja, Designing durable icephobic surfaces, Sci. Adv. 2 (2016).
[18] J.C. Bird, R. Dhiman, H.-M. Kwon, K.K. Varanasi, Reducing the contact time of a bouncing drop, Nature. 503 (2013) 385.
[19] T. Maitra, M.K. Tiwari, C. Antonini, P. Schoch, S. Jung, P. Eberle, D. Poulikakos, On the nanoengineering of superhydrophobic and impalement resistant surface textures below the freezing temperature, Nano Lett. 14 (2014) 172–182.
[20] Y. Li, B. Li, X. Zhao, N. Tian, J. Zhang, Totally waterbornenonfluorinated, mechanically robust, and self-healing superhydrophobic coatings for actual anti-icing, ACS Appl. Mater. Interfaces. 10 (2018) 39391–39399.
[21] X. Sun, V.G. Damle, S. Liu, K. Rykaczewski, Bioinspired stimuli-responsive and antifreeze-secreting anti-icing coatings, Adv. Mater. Interfaces. 2 (2015) 1400479.
[22] A.P. Esser-Kahn, V. Trang, M.B. Francis, Incorporation of antifreeze proteins into polymer coatings using site-selective bioconjugation, J. Am. Chem. Soc. 132 (2010) 13264–13269.
[23] Y. Zhang, K. Liu, K. Li, V. Gutowski, Y. Yin, J. Wang, Fabrication of anti-icing surfaces by short α-helical peptides, ACS Appl. Mater. Interfaces. 10 (2018) 1957–1962.
[24] R. Drori, C. Li, C. Hu, P. Raiteri, A.L. Rohl, M.D. Ward, B. Kahr, A supramolecular ice growth inhibitor, J. Am. Chem. Soc. 138 (2016) 13396–13401.
[25] K. Liu, C. Wang, J. Ma, G. Shi, X. Yao, H. Fang, Y. Song, J. Wang, Janus effect of antifreeze proteins on ice nucleation, PNAS. 113 (2016) 14739–14744.
[26] S.B. Subramanyam, K. Rykaczewski, K.K. Varanasi, Ice adhesion on lubricant-impregnated textured surfaces, Langmuir. 29 (2013) 13414–13418.
[27] P. Irajizad, M. Hasnain, N. Farokhnia, S.M. Sajadi, H. Ghasemi, Magnetic slippery extreme icephobic surfaces, Nat. Commun. 7 (2016) 13395.
[28] C. Stamatopoulos, J. Hemrle, D. Wang, D. Poulikakos, Exceptional anti-icing performance of self-impregnating slippery surfaces, ACS Appl. Mater. Interfaces. 9 (2017) 10233–10242.
[29] S. Zhang, J. Huang, Y. Cheng, H. Yang, Z. Chen, Y. Lai, Bioinspired surfaces with superwettability for anti-icing and ice-phobic application: concept, mechanism, and design, Small 13 (2017) 1701867.
[30] S. Zheng, D.A. Bellido-Aguilar, X. Wu, X. Zhan, Y. Huang, X. Zeng, Q. Zhang, Z. Chen, Durable waterborne hydrophobic bio-epoxy coating with improved anti-icing and self-cleaning performance, ACS Sustainable Chem. Eng. 7 (2019) 641–649.
[31] Y. Shen, X. Wu, J. Tao, C. Zhu, Y. Lai, Z. Chen, Icephobic materials: Fundamentals, performance evaluation, and applications, Prog. Mater. Sci. 103 (2019) 509–557.
[32] S. Jung, M.K. Tiwari, N.V. Doan, D. Poulikakos, Mechanism of supercooled droplet freezing on surfaces, Nat. Commun. 3 (2012) 615.
[33] J. Chen, J. Liu, M. He, K. Li, D. Cui, Q. Zhang, X. Zeng, Y. Zhang, J. Wang, Y. Song, Superhydrophobic surfaces cannot reduce ice adhesion, Appl. Phys. Lett. 101 (2012) 111603.
[34] K. Li, S. Xu, W. Shi, M. He, H. Li, S. Li, X. Zhou, J. Wang, Y. Song, Investigating the effects of solid surfaces on ice nucleation, Langmuir. 28 (2012) 10749–10754.
[35] P.L. Davies, Ice-binding proteins: a remarkable diversity of structures for stopping and starting ice growth, Trends Biochem. Sci. 39 (2014) 548–555.
[36] Y. Yu, B. Jin, M.I. Jamil, D. Cheng, Q. Zhang, X. Zhan, F. Chen, Highly stable amphiphilic organogel with exceptional anti-icing performance, ACS Appl. Mater. Interfaces 11 (2019) 12838–12845.
[37] J.S. Zigmond, A. Pavía-Sanders, J.D. Russell, K.L. Wooley, Dynamic anti-icing coatings: complex, amphiphilic hyperbranched fluoropolymer poly(ethylene glycol) cross-linked networks with an integrated liquid crystalline comonomer, Chem. Mater. 28 (2016) 5471–5479.
[38] C. Li, X. Li, C. Tao, L. Ren, Y. Zhao, S. Bai, X. Yuan, Amphiphilic antifogging/anti-icing coatings containing POSS-PDMAEMA-b-PSBMA, ACS Appl. Mater. Interfaces 9 (2017) 22959–22969.
[39] V. Upadhyay, T. Galhenage, D. Battocchi, D. Webster, Amphiphilic icephobic coatings, Prog. Org. Coat. 112 (2017) 191–199.
[40] J.S. Zigmond, K.A. Pollack, S. Smedley, J.E. Raymond, L.A. Link, A. Pavía-Sanders, M.A. Hickner, K.L. Wooley, Investigation of intricate, amphiphilic crosslinked hyperbranched fluoropolymers as anti-icing coatings for extreme environments, J. Polym. Sci. Part A: Polym. Chem. 54 (2016) 238–244.
[41] E. Pouget, J. Tonnar, P. Lucas, P. Lacroix-Desmazes, F.o. Ganachaud, B. Boutevin, Well-architectured poly (dimethylsiloxane)-containing copolymers obtained by radical chemistry, Chem. Rev. 110 (2009) 1233-1277.
[42] G. Momen, M. Farzaneh, R. Jafari, Wettability behaviour of RTV silicone rubber coated on nanostructured aluminium surface, Appl. Surf. Sci. 257 (2011) 6489–6493.
[43] P.K. Jain, X. Huang, I.H. El-Sayed, M.A. El-Sayed, Noble metals on the nanoscale: optical and photothermal properties and some applications in imaging, sensing, biology, and medicine, Acc. Chem. Res. 41 (2008) 1578–1586.
[44] R. Yoshikawa, M. Tenjimbayashi, S. Shiratori, Electrothermally triggered broadband optical switch films with extremely low power consumption, ACS Appl. Energ. Mater. 1 (2018) 1429–1434.
[45] A. Guo, X. Ming, Y. Fu, G. Wang, X. Wang, Fiber-based, double-sided, reduced graphene oxide films for efficient solar vapor generation, ACS Appl. Mater. Interfaces. 9 (2017) 29958–29964.
[46] H. Guo, J. Yang, T. Xu, W. Zhao, J. Zhang, Y. Zhu, C. Wen, Q. Li, X. Sui, L. Zhang, A robust cotton textile-based material for high-flux oil-water separation, ACS Appl. Mater. Interfaces. 11 (2019) 13704–13713.
[47] A.J. Meuler, J.D. Smith, K.K. Varanasi, J.M. Mabry, G.H. McKinley, R.E. Cohen, Relationships between water wettability and ice adhesion, ACS Appl. Mater. Interfaces. 2 (2010) 3100–3110.
[48] H. Cong, L. Li, S. Zheng, Poly (N-isopropylacrylamide)-block-poly (vinyl pyrrolidone) block copolymer networks: Synthesis and rapid thermoresponse of hydrogels, Polymer. 54 (2013) 1370–1380.
[49] H. Guo, J. Yang, W. Zhao, T. Xu, C. Lin, J. Zhang, L. Zhang, Direct formation of amphiphilic crosslinked networks based on PVP as a marine anti-biofouling coating, Chem. Eng. J. 374 (2019) 1353–1363.
[50] M. Liu, X. Zhang, H. Guo, Y. Zhu, C. Wen, X. Sui, J. Yang, L. Zhang, Dimethyl sulfoxide-free cryopreservation of chondrocytes based on zwitterionic molecule and polymers, Biomacromolecules. 20 (2019) 3980–3988.
[51] X. Sui, C. Wen, J. Yang, H. Guo, W. Zhao, Q. Li, J. Zhang, Y. Zhu, L. Zhang, Betaine combined with membrane stabilizers enables solvent-free whole blood cryopreservation and one-step cryoprotectant removal, ACS Biomater. Sci. Eng. 5 (2019) 1083–1091.
[52] J. Yang, C. Pan, J. Zhang, X. Sui, Y. Zhu, C. Wen, L. Zhang, Exploring the potential of biocompatible osmoprotectants as highly efficient cryoprotectants, ACS Appl. Mater. Interfaces. 9 (2017) 42516–42524.
[53] T.-S. Wong, S.H. Kang, S.K.Y. Tang, E.J. Smythe, B.D. Hatton, A. Grinthal, J. Aizenberg, Bioinspired self-repairing slippery surfaces with pressure-stable omniphobicity, Nature. 477 (2011) 443.
[54] T. Cheng, R. He, Q. Zhang, X. Zhan, F. Chen, Magnetic particle-based super-hydrophobic coatings with excellent anti-icing and thermoresponsive deicing performance, J. Mater. Chem. A. 3 (2015) 21637–21646.
[55] R. Dou, J. Chen, Y. Zhang, X. Wang, D. Cui, Y. Song, L. Jiang, J. Wang, Anti-icing coating with an aqueous lubricating layer, ACS Appl. Mater. Interfaces. 6 (2014) 6998–7003.
[56] A. Kirillova, L. Ionov, I.V. Roisman, A. Synytska, Hybrid hairy janus particles for anti-icing and de-icing surfaces: synergism of properties and effects, Chem. Mater. 28 (2016) 6995–7005.
[57] F. Arianpour, M. Farzaneh, S.A. Kulinich, Hydrophobic and ice-retarding properties of doped silicone rubber coatings, Appl. Surf. Sci. 265 (2013) 546–552.
[58] H. Li, X. Li, C. Luo, Y. Zhao, X. Yuan, Icephobicity of polydimethylsiloxane-b-poly (fluorinated acrylate), Thin Solid Films. 573 (2014) 67–73.
[59] X. Li, Y. Zhao, H. Li, X. Yuan, Preparation and icephobic properties of polymethyltrifluoropropylsiloxane–polyacrylate block copolymers, Appl. Surf. Sci. 316 (2014) 222–231.
[60] A. Davis, Y.H. Yeong, A. Steele, I.S. Bayer, E. Loth, Superhydrophobic nanocomposite surface topography and ice adhesion, ACS Appl. Mater. Interfaces. 6 (2014) 9272–9279.
[61] M. Susoff, K. Siegmann, C. Pfaffenroth, M. Hirayama, Evaluation of icephobic coatings—Screening of different coatings and influence of roughness, Appl. Surf. Sci. 282 (2013) 870–879.
[62] Y. He, C. Jiang, X. Cao, J. Chen, W. Tian, W. Yuan, Reducing ice adhesion by hierarchical micro-nano-pillars, Appl. Surf. Sci. 305 (2014) 589–595.
[63] L. Zhu, J. Xue, Y. Wang, Q. Chen, J. Ding, Q. Wang, Ice-phobic coatings based on silicon-oil-infused polydimethylsiloxane, ACS Appl. Mater. Interfaces. 5 (2013) 4053–4062.
[64] E.J.Y. Ling, V. Uong, J.-S. Renault-Crispo, A.-M. Kietzig, P. Servio, Reducing ice adhesion on nonsmooth metallic surfaces: wettability and topography effects, ACS Appl. Mater. Interfaces. 8 (2016) 8789–8800.
[65] S. Chernyy, M. Järn, K. Shimizu, A. Swerin, S.U. Pedersen, K. Daasbjerg, L. Makkonen, P. Claesson, J. Iruthayaraj, Superhydrophilic polyelectrolyte brush layers with imparted anti-icing properties: effect of counter ions, ACS Appl. Mater. Interfaces. 6 (2014) 6487–6496.
[66] L. Foroughi Mobarakeh, R. Jafari, M. Farzaneh, The ice repellency of plasma polymerized hexamethyldisiloxane coating, Appl. Surf. Sci. 284 (2013) 459–463.
[67] X. Yin, Y. Zhang, D. Wang, Z. Liu, Y. Liu, X. Pei, B. Yu, F. Zhou, Integration of self-lubrication and near-infrared photothermogenesis for excellent anti-icing/deicing performance, Adv. Funct. Mater. 25 (2015) 4237–4245.
[68] J. Chen, Z. Luo, Q. Fan, J. Lv, J. Wang, Anti-ice coating inspired by ice skating, Small. 10 (2014) 4693–4699.
[69] Y. Shen, H. Tao, S. Chen, L. Zhu, T. Wang, J. Tao, Icephobic/anti-icing potential of superhydrophobic Ti6Al4V surfaces with hierarchical textures, RSC Adv. 5 (2015) 1666–1672.
[70] X. Deng, L. Mammen, H.-J. Butt, D. Vollmer, Candle soot as a template for a transparent robust superamphiphobic coating, Science. 335 (2012) 67–70.
[71] C.-H. Xue, Z.-D. Zhang, J. Zhang, S.-T. Jia, Lasting and self-healing superhydrophobic surfaces by coating of polystyrene/SiO_2 nanoparticles and polydimethylsiloxane, J. Mater. Chem. A. 2 (2014) 15001–15007.